Thin–Walled Structures 226 (2026) 114901

Contents lists available at ScienceDirect

Thin-Walled Structures

journal homepage: www.elsevier.com/locate/tws

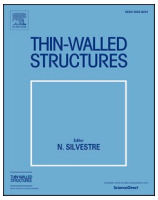

Full length article

Shear fatigue life of injected bolted connectors in GFRP sandwich web core panels: Effects of load ratio and aging

Angeliki Christoforidou, Abishek Baskar, Marko Pavlovic *

Steel and Composite Structures, Department of Engineering Structures, Faculty of Civil Engineering and Geosciences, Delft University of Technology, Stevinweg 1, Delft, 2628 CN, South Holland, the Netherlands

ARTICLE INFO

Keywords:
Injected steel reinforced resin connectors
Fatigue
Water immersion
Experimental characterization
Sandwich structures
FRP materials and structures

ABSTRACT

The durability of bridge connections is critical for the long-term performance of bridge systems with GFRP composite decks. This study investigates the shear fatigue behaviour of injected Steel Reinforced Resin (iSRR) connectors embedded in FRP composite decks, through a series of fatigue tests performed under different load ratios and exposure conditions. Twenty-four connectors are examined: twelve unaged reference specimens, eight specimens tested under varying *R* ratios, two connectors with deck parts submerged in water and two subjected to outdoor aging, both for a duration of one year. The results show that, despite the composite nature of the connector, the load ratio and mean load level have minimal influence on fatigue life. Instead, fatigue performance in the high-cycle regime is governed primarily by the applied load range. A unified *F-N* curve including all *R* ratios was developed, demonstrating the consistency of this trend and enabling fatigue-life prediction across different loading conditions. Environmental exposure led to measurable stiffness degradation but did not significantly alter fatigue life. These findings highlight the robustness of the iSRR connector and support its application in durable GFRP-steel hybrid bridge systems.

1. Introduction

Highway bridge infrastructure is ageing worldwide, and many existing bridges are increasingly unable to accommodate present-day traffic volumes, axle loads and environmental exposure. These factors accelerate fatigue and corrosion processes, particularly in reinforced-concrete bridge decks Across Europe, a large proportion of the motorway network was designed using historic traffic and load models that are now clearly exceeded in practice [1]. Recent assessments in Germany and the Netherlands have identified thousands of bridges in poor or inadequate condition, often requiring major strengthening measures or complete deck replacement to maintain acceptable safety and serviceability levels [2–4].

At the same time, bridge owners are facing growing societal and political pressure to limit traffic disruption and to reduce the embodied carbon associated with infrastructure interventions. As a result, there has been a noticeable shift away from full bridge replacement towards rehabilitation strategies that aim to extend service life while improving load-carrying capacity and long-term durability [5]. Within this context, bridge decks play a particularly important role. Being directly exposed to mechanical fatigue, de-icing salts, moisture ingress and temperature variations, decks often govern the residual capacity and serviceability performance of existing highway bridges [6,7].

Composite bridge decks made from Glass Fibre Reinforced Polymer (GFRP) sandwich panels have been proposed and, in some cases, implemented as an alternative to conventional concrete decks. Their low self-weight, inherent corrosion resistance and favourable fatigue behaviour make them attractive for bridge rehabilitation projects, while also reducing maintenance demands over the service life [8,9]. Numerous studies on FRP bridge decks and hybrid FRP-steel systems have shown that such solutions can restore or even increase live-load capacity while allowing existing substructures to be reused. This enables rapid installation, minimises traffic closures and supports design service lives that are comparable to, or longer than, those of traditional deck systems [10,11]. Practical applications, including systems developed within research initiatives such as SUREbridge [12,13] as well as several proprietary FRP deck products [14], demonstrate that GFRP decks can be successfully integrated in both new construction and rehabilitation projects, particularly where weight reduction and durability are key design drivers.

* Corresponding author.
E-mail address: m.pavlovic@tudelft.nl (M. Pavlovic).

https://doi.org/10.1016/j.tws.2026.114901
Received 30 January 2026; Received in revised form 19 March 2026; Accepted 30 March 2026
Available online 1 April 2026

Despite these advantages, the introduction of GFRP deck systems into existing steel or concrete superstructures raises a critical challenge: the development of a reliable, durable and practical connection between the composite deck and the supporting structure. To address this issue, a novel connector concept, referred to as the injected Steel Reinforced Resin (iSRR) connector, was introduced in [15]. The iSRR system combines conventional steel rods or bolts with an injected steel-reinforced resin (SRR), consisting of steel shot embedded in a polymer resin. The SRR is injected into a relatively large cylindrical hole in the composite deck, fully surrounding the mechanical connector, as illustrated in Fig. 1. This configuration leads to a more favourable distribution of bearing stresses and eliminates slip through preloading of the steel connector against the steel flange. Importantly, the GFRP laminate itself is kept outside the preload zone, while load transfer is carried primarily by the SRR-encased steel connector, making the system particularly suited for bridge rehabilitation applications using composite panels.

Existing research on iSRR connectors has mainly focused on static strength, slip behaviour and fatigue performance under a single stress ratio and standard laboratory climate conditions. More recently, some studies have also investigated stiffness evolution and fatigue life at elevated temperatures representative of hot-weather exposure [16,18,19]. Overall, these studies indicate that injected connectors can maintain favourable load-transfer characteristics and stable fatigue behaviour up to moderately elevated temperatures, provided that the resin system remains below its glass-transition temperature. For example, previous fatigue tests on iSRR connectors reported *F-N* curve inverse slope parameters of $m = -6.6$ at room temperature and $m = -5.8$ at elevated temperature [16]. In addition, durability studies on resin-based anchorage systems and GFRP-resin assemblies have shown good performance under freeze-thaw cycling and low-temperature exposure, with only limited reductions in stiffness and strength, suggesting that cold climates are unlikely to govern the performance of such connections [20,21].

By contrast, moisture ingress and prolonged exposure to high humidity are known to influence polymer matrices and bonded interfaces. However, their effect on the mechanical response and fatigue performance of iSRR connectors used in GFRP bridge decks has not yet been systematically investigated. In addition, the influence of the applied stress ratio R on fatigue life and stiffness degradation under realistic traffic-type loading conditions remains largely unexplored. In the present paper these gaps are addressed through an experimental study on

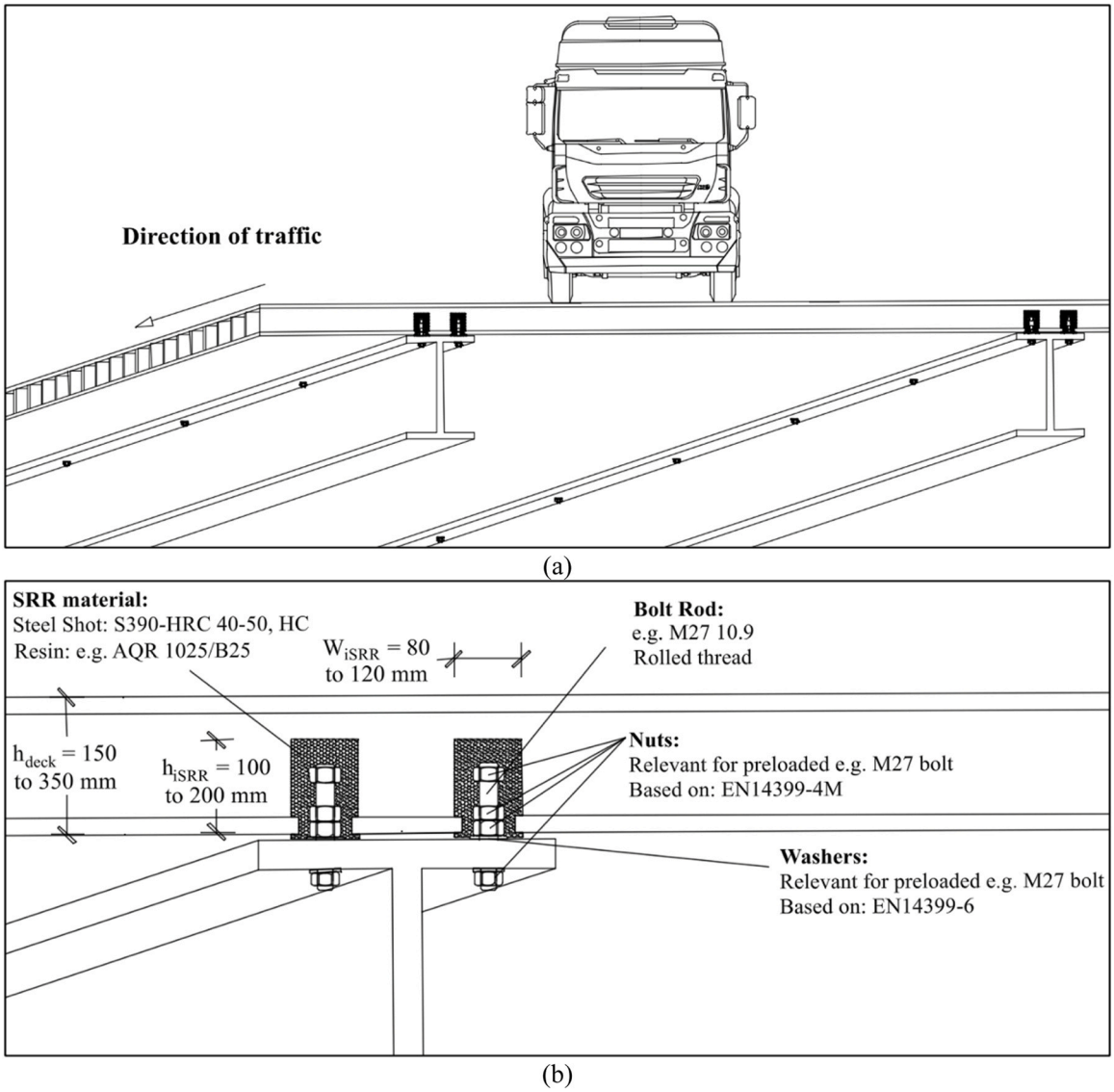

Fig. 1. Cross section of a bridge with iSRR bolted connections between composite deck panel and steel girder: (a) Global view, (b) Close-up view of iSRR connectors [16,17].

iSRR connectors, focusing on the combined effects of stress ratio and moisture exposure. The investigation includes measurements of stiffness evolution, slip behaviour, failure modes and fatigue life for iSRR connections tested under different stress ratios and environmental conditions.

2. Description of experimental campaign

2.1. Details of specimens and materials

The key dimensions of the test specimens and the assembly of the iSRR connectors are depicted in Fig. 2. The full connector configuration is illustrated in Fig. 2(b) and consists of an M27 bolt rod, embedded nuts, washers, and a SRR injection piece. The SRR material consists of S390 steel shot (HRC 40–50) mixed with an unsaturated polyester polyurethane resin (AQR 1025/B25) at defined proportions. It can be seen in Fig. 2(b) that the SRR piece does not extend to the top of the washer, so that the preload path involves only metallic components and is not affected by resin-based materials. The selection of the M27 bolt is based on analysis of thermal load effects under serviceability conditions in a hybrid GFRP-steel bridge deck system. High longitudinal forces near the cross- to main-girder connections led to a satisfactory unity check when using M27 bolt rods [22]. All the material properties of the components from the testing campaign are provided in Table 1.

The iSRR connectors were embedded in GFRP sandwich web-core panels manufactured by FiberCore Europe using vacuum infusion. The panels consist of continuous 1.27 m wide glass fibre fabrics and polyurethane foam cores without splices to minimize resin accumulation and potential distortion. Each core is wrapped with ±45° fabrics to promote shear continuity between the skins and the integrated webs. To facilitate this monolithic construction, a continuous "Z-shape" wrapping technique is employed, which results in the non-symmetrical stacking sequences incorporating an inclined layup configuration where the web fabrics transition diagonally between the facings [14].

In a full-scale bridge deck, the primary reinforcement is typically oriented in the longitudinal span direction, parallel to the webs, to provide bending stiffness. However, the component-level specimens in this study were oriented such that the loading axis is perpendicular to the webs. Consequently, the local 0° direction (parallel to the load) contains 10 laminae, while the 90° direction (perpendicular to the load,

Table 1
Material properties of the connector and decks components.

Component	Mechanical properties
UD laminate[15]	$E_1 = 31450$ MPa, $E_2 = E_3 = 8459$ MPa, $G_{12} = G_{13} = 4838$ MPa $G_{23} = 3021$ MPa, $\nu_{12} = \nu_{13} = 0.272$, $\nu_{23} = 0.4$, $\rho = 1873$ kg/m3
Foam[23]	$E = 2.1$ MPa, $\nu = 0.3$, $\rho = 32$ kg/m3
Steel shot[24]	S390, HRC 40–50, $\rho = 7400$ kg/m3
Resin[25]	$\eta = 150$ - 220 [mPa.s], $E = 3530$ MPa, $T_g = 135$ °C
SRR[26,27]	$E_t = 16181$ MPa, $f_t = 10$ MPa, $\nu = 0.13$ and $\rho = 4955$ kg/m3
M27 Bolt rod	Grade 10.9, $E = 210000$ MPa, $\nu = 0.3$, S355
M27 Nuts & Washers	Grade 10.9, $E = 210000$ MPa, $\nu = 0.3$, S355

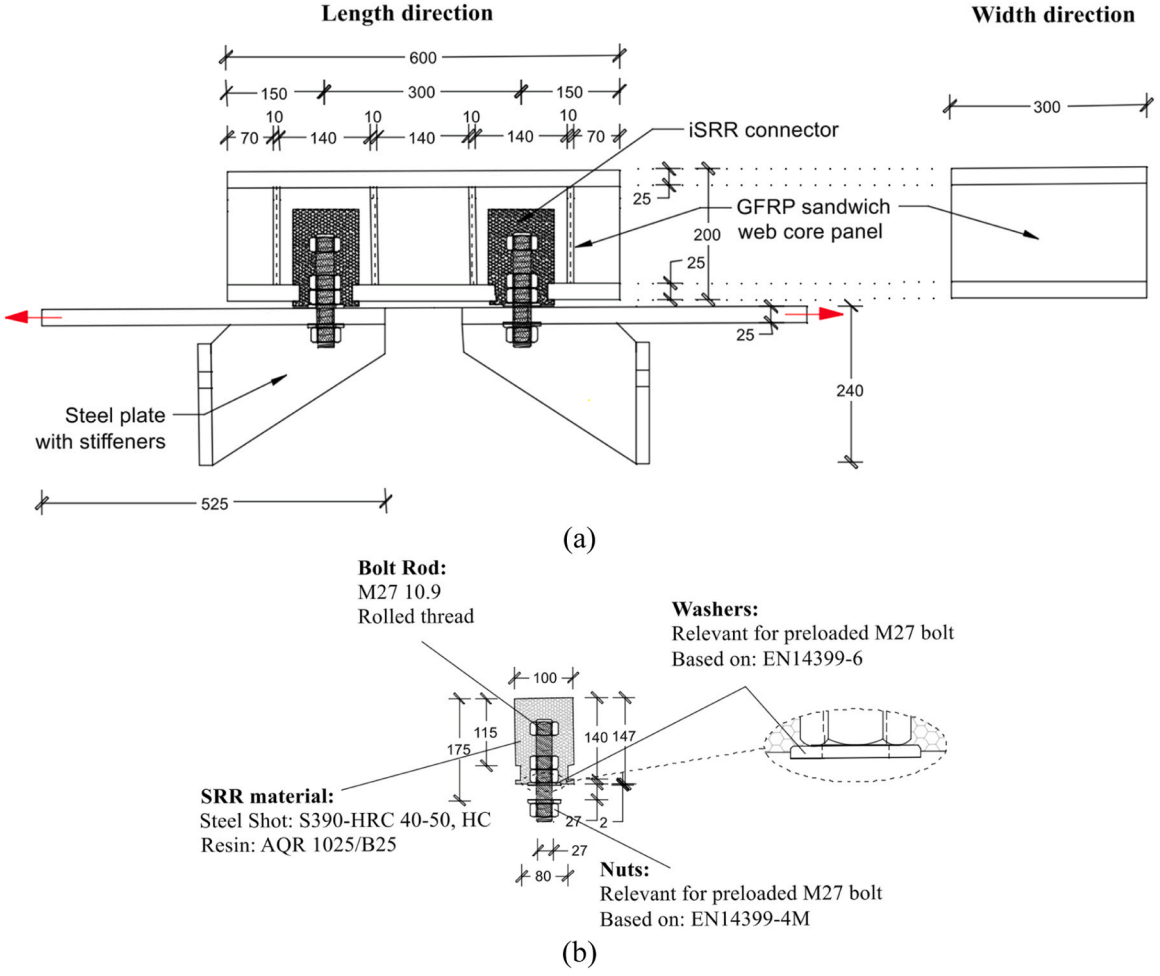

Fig. 2. iSRR connectors in composite-steel single-lap shear joint specimens (dimensions in mm): (a) Detailed view of configuration (red arrows indicate loading direction), (b) Details of the connector [16,17].

representing the global span direction) contains 22 laminae. This configuration ensures the tests accurately capture the transverse stiffness and shear transfer mechanisms typical of Dutch infrastructure. The facings have a total thickness of 25 mm, and the webs are spaced at 150 mm centre-to-centre with a nominal thickness of 10 mm. The final stacking sequences follow CUR recommendations and are presented in Table 2 [28].

2.2. Test setup and instrumentation

The iSRR connectors are slip resistant due to the inclusion of the SRR resin that surrounds the bolt rod in the oversized hole making sure that nothing moves in the FRP bottom facing. However, the bolt rod passes through the hole of the steel girder which in these experimental set up is represented by the steel end details clamped in the machine. Thus, prior to the initiation of the cyclic loading all connectors preload with a torque level of 1350 Nm is then applied to the bolts using a calibrated torque gun only after the specimen is placed within the steel loading frame. As the clamping package consists only of metallic components, no significant preload loss due to creep is expected, and the fatigue response is governed by the SRR-GFRP interface rather than by bolt slip, provided that the applied shear forces remain below the slip resistance.

The experimental set-up, including the test specimen and the test rig, is shown in Fig. 3. The cyclic shear test configuration adopted in this study follows a dedicated setup-development study [17] in which different boundary conditions and specimen configurations were evaluated numerically in order to obtain a connector-level test arrangement that reproduces realistic shear load transfer in hybrid steel-GFRP bridges. In that work, a complementary bridge-scale model with an FRP deck and iSRR connectors was also developed to quantify connector force levels and to benchmark the connector-region stress distribution; similar stress concentration regions were identified in the SRR-GFRP interface and beneath the nut/washer for comparable connector shear forces.

An Instron dual column testing equipment with a load cell capacity of 600 kN is utilized. Part of the steel end detail is clamped in the hydraulic jaws, whilst their horizontal elements are fastened to the upper and (movable) lower cross heads. The displacement range increase is measured using Linear Variable Differential Transducers (LVDTs) that track the relative movement between the GFRP bottom facing and the steel end detail. The LVDTs are attached with their moving part positioned on the GFRP facing and their fixed bracket on the steel detail. By recording the change in relative displacement during each cycle, the total displacement range increase of the iSRR connectors can be evaluated, allowing for an accurate assessment of fatigue-related deformation over time. The exact same test set up was also utilized in prior study, where the influence of load levels was examined under fully reversed cyclic loading [16].

2.3. Test matrix

A total of six specimens, comprising twelve connectors, are prepared and tested, following a specific naming convention: X-YY-ZZ-E-D-C. The first character (X) represents the type of loading, which can either be “S” for the post cyclic Static loading or "F" for Fatigue loading. The 'YY' segment denotes the maximum applied load during the cyclic test. For fully reversed loading cases (R = −1), a single value is provided, while for non-fully reversed cases, both maximum and minimum loads are indicated. For instance, an *R* ratio of 0.5 with a maximum load of 80 kN would be represented as 80_40. The letters (ZZ) denote the testing temperature, which remains constant at room temperature (RT) in this study. The letter (E) indicates the exposure condition: "U" for unaged, "S" for submerged in water, and "O" for outdoor exposure. The digit (D) refers to the specimen count for each parameter combination (X, YY, ZZ, E), which can be either 1 or 2. Lastly, the letter (C) designates the connector location within the panel, with "T" for top and "B" for bottom.

Table 2
Stacking sequence of laminates of GFRP deck; 0° denotes the local loading direction; 90° denotes the direction perpendicular to the load (global span direction).

Facings (skins)	Webs
[45/−45/45/−45/45/−45/0_2/90_2/45/−45/90_3/0_2/90_2/45/−45/90_3/0_2/90_2/45/−45/90_3/0_2/90_2/45 /−45/90_3/0_2/90_2/45/−45]	[−45/45/−45/45/−45/45/−45/45/90_2/0_2/−45/45/−45/45/−45/45]

Unlike previous studies, different *R* ratios will be applied in this investigation to assess their effect on the fatigue performance of the connectors and expand the understanding of load ratio influence on the fatigue behavior of the iSRR connectors. Two additional *R* ratios, *R* = 0.5 and *R* = 0.1, are examined, with maximum load levels of 80 kN and 100 kN applied for each *R* ratio. Regarding the environmental exposure, four connectors are subjected to different environmental scenarios: two submerged in water and two exposed to outdoor conditions, each for a year, as shown in Fig. 4. After this exposure, the connectors are tested under cyclic loading with a maximum load of 80 kN, and with the most detrimental *R* ratio that will be found in this study.

To relate these load levels to normal service conditions, connector forces were taken from bridge-level analyses of representative hybrid steel-GFRP bridges with iSRR connectors [29]. In the corresponding fatigue shear-force study, the characteristic shear force ranges in service were found to be of the order of 30–40 kN for connectors in the lengthwise middle of the spans and up to approximately 60 kN for connectors close to the supports, where the largest force ranges occur. Complementary static analyses for the same bridge configurations showed maximum shear forces in the bolted connectors due to traffic loading in the range 50–87 kN (with existing highway bridges managed by Dutch Ministry of Infrastructure exhibiting values between about 10 and 110 kN), and maximum shear forces due to temperature loading in the range 5–60 kN, depending on girder spacing and laminate orientation. The minimum-maximum force levels of 40–100 kN and the investigated R-ratios in the present campaign therefore span the typical service-level connector demands and extend towards the upper end of the static shear-force envelope, providing a realistic to mildly conservative representation of in-service loading for iSRR connectors in hybrid bridges.

The water immersion specimens were aged in demineralized water (without additional solvents) within the Stevin II laboratory at TU Delft. The laboratory environment was maintained at a controlled nominal temperature of 20±2 °C throughout the duration of the immersion. The outdoor specimens were exposed for a 12-month period from July 2023 to July 2024 in Delft, Netherlands. The site is characterized by a temperate oceanic climate. During the exposure window, the environmental conditions were defined by an annual mean temperature of 11.5 °C, with observed extremes ranging from −3 °C in January to 33 °C in August. The total annual precipitation was approximately 870 mm, with the highest rainfall intensity occurring during the autumn months. The mean relative humidity remained high at approximately 82%, and the total cumulative solar radiation for the period was approximately 1100 kWh/m^2 (avg. 3.0 kWh/m^2/day).

The experimental test matrix is presented in Table 3, summarizing the number of tests for each loading condition and the corresponding environmental exposure and *R* ratio applied in this study. To assess the impact of environmental exposure and *R* ratio, these experimental results from this study are compared with the reference case of four connectors tested at room temperature, subjected to fully reversed cyclic loading.

Since results from a previous test campaign are used in combination with the new tests, it is important to highlight that all specimens share the same essential characteristics. The *R* = −1 reference tests, taken from [16], were performed on specimens cut from the same

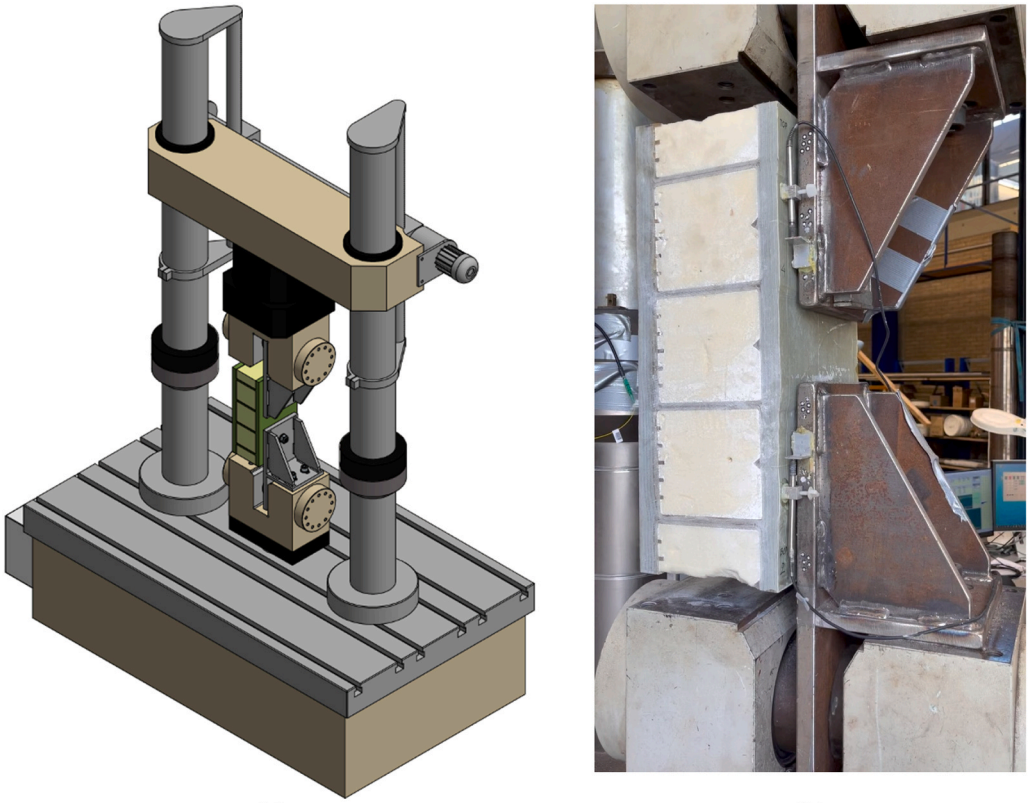

Fig. 3. Test set-up: (a) schematic representation of test arrangement, (b) realised experimental set-up.

Fig. 4. iSRR connectors subjected to water exposure: (a) Submerged connectors, (b) Outdoors exposure.

Table 3
Overview of experiments for SRR material characterization under compression.

Maximum load [kN]	R ratio [-]	Environmental exposure	Number of connectors
40*	−1	No exposure	4
60*	−1	No exposure	4
80*	−1	No exposure	4
80	0.1	No exposure	2
100	0.1	No exposure	2
80	0.5	No exposure	2
100	0.5	No exposure	2
80	−1	Outdoors	2
80	−1	Submerged	2

* Results taken from [16]

vacuum-infused GFRP sandwich deck used in the present work, with identical laminate configuration, connector detailing, specimen geometry, loading protocol, measurement setup and fatigue-life estimation procedure as in the present campaign; only the iSRR connectors were injected on different days, following the exact same procedure. Consequently, no systematic differences in testing conditions are expected, and the datasets can be directly combined in the unified analysis presented in the following sections.

2.4. Stop and failure criterion

The stop criteria adopted in this study follow the constraints of the experimental campaign and the expected behaviour of the iSRR

connector under different conditions. A cycle-based stop criterion is applied for all tests where failure is not anticipated within a practical timeframe. This limit is introduced based on experience from fully reversed tests at $R = -1$ reported in [16], corresponding to 1.50E + 06 cycles. For the tests conducted at $R = 0.1$ and $R = 0.5$, failure is not expected due to the substantially smaller total force range. These specimens are therefore cycled up to the predefined stop criterion, while the evolution of stiffness degradation is monitored and later compared to the reference behaviour at $R = -1$ from [16]. In these cases, the objective is not to reach failure but to characterise and compare degradation trends.

For the environmentally exposed connectors, a different response is observed. After one year of outdoor or submerged aging and subsequent cyclic loading at ±80 kN, which is the most detrimental condition identified previously, the specimens did reach failure. In this study, failure is defined as fracture of the connector during cyclic loading, and this criterion governs the termination of these tests. The cycle-based stop limit applies only if no failure occurs; however, for the aged specimens, fracture consistently occurred before reaching this limit. An overview of the termination criteria is presented in Table 4.

3. Experimental results and observations

3.1. Evolution of displacement range under different load ratios

3.1.1. Displacement range increase

Results of displacement range increase for tests conducted at different load ratios R but with same maximum load (80 kN) are presented in Fig. 5. The inclusion of both linear, in Fig. 5(a), and logarithmic scale axes, in Fig. 5(b), is intended to help the reader clearly see and interpret these differences. The graphs compare the cyclic tests conducted at fully reversed loading $R = -1$, with tests at lower load ranges for $R = 0.1$ and $R = 0.5$. It is evident that the displacement range increase for $R = 0.5$ and $R = 0.1$ tests is significantly lower than for the alternating load ratio $R = -1$. This suggests that the load ratio strongly influences fatigue damage, with non-alternating load ratios $R = 0.1$ and $R = 0.5$ showing much less stiffness degradation.

Furthermore, Fig. 6(a) and Fig. 6(b) present test results with different maximum loads and load ratios but comparable load ranges using two different scale axes. The figures include results of cyclic tests at minimum-to-maximum loads of 10–100 kN, 8–80 kN, and −40 to + 40 kN, corresponding to load ranges of 90 kN, 72 kN, and 80 kN, respectively. The displacement range increase is of comparable magnitude for the three cases, with the alternating load case exhibiting the most significant degradation. This observation partially supports the initial hypothesis that the alternating load ($R = -1$) is the most detrimental when considered for a given load range. Furthermore, these results highlight that it is not the maximum load alone but rather the load range that governs the damage rate and, consequently, the fatigue life of the connectors.

3.1.2. Failure modes after post-cyclic monotonic and cyclic loading

Following the completion of 1.50E + 06 cycles, none of the specimens tested at $R = 0.1$ and $R = 0.5$ exhibited fatigue failure, consistent with the limited displacement-range increase observed in Section 3.1.1.

Table 4
Termination criteria for assessing influence of load ratio and aging effects.

Environmental exposure	R ratio	Failure criterion
No exposure	0.1	No. cycles exceeding 1.50E + 06[1]
No exposure	0.5	No. cycles exceeding 1.50E + 06[2]
Outdoors	−1	Failure
Submerged	−1	Failure

1) Tested under monotonic loading after cyclic tests (post-cyclic static loading)

2) Tested under ±80 kN cyclic loading to failure after initial cyclic tests

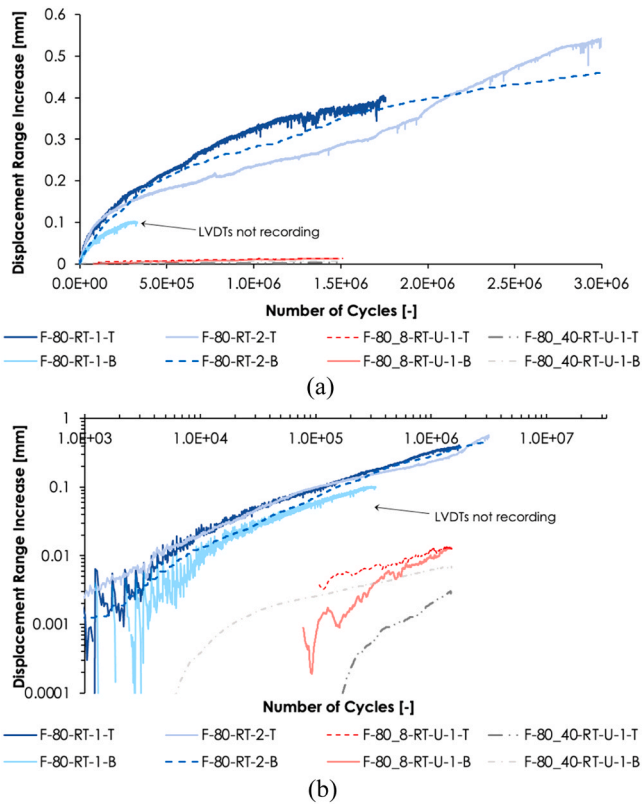

Fig. 5. Displacement range increase of different R ratios with maximum force of 80 kN: (a) Linear scale axes, (b) Logarithmic scale axes; Colour gradients indicate the R ratio: blue for $R = -1$, red for $R = 0.1$, black for $R = 0.5$.

The minimal stiffness degradation at both load ratios indicates that the applied cyclic force ranges were insufficient to trigger progressive damage leading to failure within the prescribed number of cycles. To characterise the ultimate failure behaviour of these connectors, additional tests were performed after the cyclic loading stage. The specimens tested at $R = 0.1$ were subsequently subjected to monotonic loading to failure, while those tested at $R = 0.5$, which showed almost no measurable degradation, were reloaded under fully reversed cyclic loading until failure occurred.

The ultimate load behavior of the specimens tested at $R = 0.1$ is assessed through monotonic loading to failure. Representative force-displacement curves obtained from these post-cyclic static tests are shown in Fig. 7. Despite the prior cyclic loading, the connectors developed a response comparable in shape to that observed in earlier fully reversed studies, characterized by an initial linear regime, followed by slip initiation, and a secondary hardening phase leading to ultimate load [16]. Both specimens display similar peak resistance of 228 kN and 235 kN for the 100 kN and 80 kN maximum cyclic loading. The resulting curves also indicate that the fatigue history at $R = 0.1$ produced a reduction within the expected variability in ultimate capacity and deformation capacity, confirming that the displacement-range evolution observed during cycling did not induce significant damage.

The connectors tested at $R = 0.5$ exhibit minimal stiffness degradation, with an increase in displacement range limited to approximately 0.05 mm after 1.50E + 06 loading cycles. This suggests that the connectors retain significant residual strength, prompting further tests to assess their capacity under more detrimental fatigue conditions. The subsequent tests are conducted at a maximum load of ±80 kN with a load ratio of $R = -1$ which represents the most damaging fatigue scenario, to evaluate the ultimate failure behaviour of the previously cycled connectors.

The new results correspond to specimens 3 and 4 and are presented

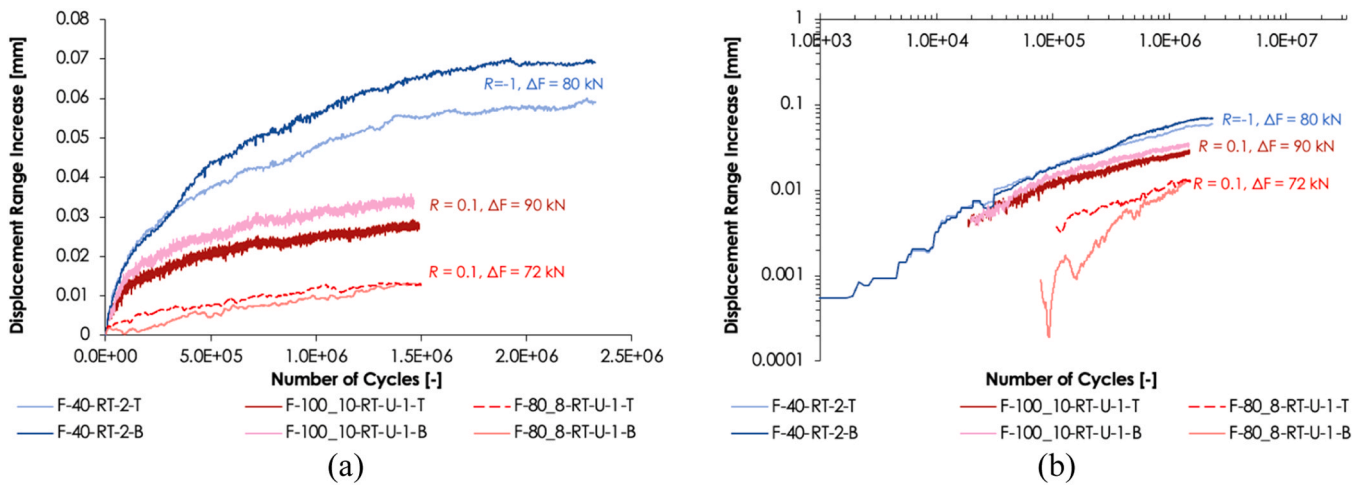

Fig. 6. Displacement range increase of different R ratio with comparable load ranges: (a) Linear scale axes, (b) Logarithmic scale axes; Colour gradients indicate the R ratio: blue for $R = -1$, red for $R = 0.1$.

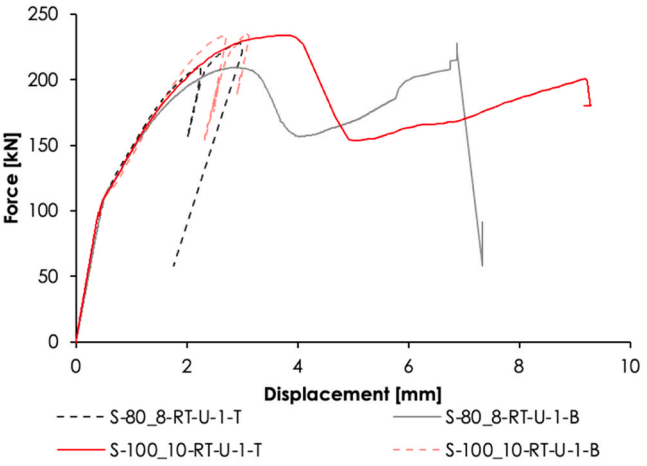

Fig. 7. Force-displacement curves of iSRR connectors under post-cyclic ($R = 0.1$) static loading.

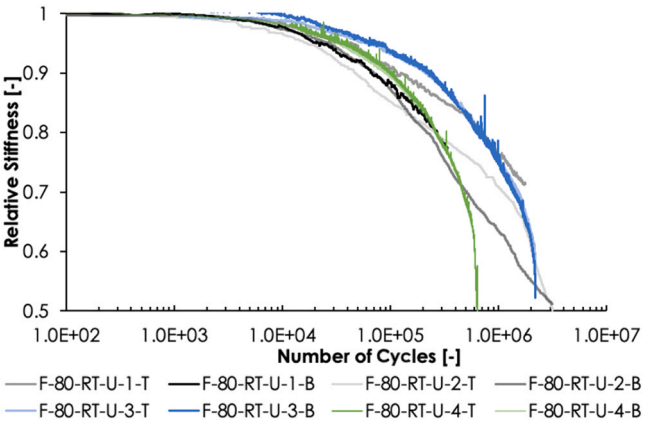

Fig. 8. Relative stiffness of iSRR connector at fully reversed cyclic load of maximum 80 kN.

in Fig. 8, which illustrates the stiffness degradation curves of the re-tested connectors under $R = -1$. The connectors previously tested under $R = -1$ without prior cycling at $R = 0.5$ are also plotted in black/grey scale alongside as a reference. Notably, the stiffness degradation trends of the re-tested connectors align closely with those of the reference specimens, suggesting that the residual strength of the connectors is substantial even after extended cycling at $R = 0.5$. However, a key difference emerges in the final stage of testing, where the re-tested specimens exhibit actual failure at a displacement threshold, whereas the virgin specimens display a more gradual stiffness degradation. This shift in behaviour between the virgin and re-tested specimens occurs beyond the adopted "apparent" failure criterion of an additional displacement range increase of 0.3 mm, highlighting that despite initial similarities in stiffness trends, the re-tested specimens eventually reach a distinct failure mode.

The re-tested specimens fail approximately after 2.00E + 06 after reaching 0.95 mm of additional displacement range increase. In terms of failure mode, debonding between the SRR piece and the GFRP facing, along with crushing of the SRR material beneath the embedded nuts is observed, as shown in Fig. 9. These results offer insight into the

Fig. 9. Failure mode of re-tested iSRR connector subjected to fully reversed cyclic loading.

connectors' durability under varying fatigue conditions, demonstrating their ability to endure substantial cycling without major degradation when initially tested at less severe load ratios.

Overall, the nearly unchanged post-cyclic force-displacement curves at $R = 0.1$ and the close match between the stiffness-degradation trends of re-tested R = 0.5 specimens and virgin $R = -1$ specimens indicate that positive R-ratio loading up to 1.50E + 06 cycles primarily causes limited interface-related damage and slip accumulation, rather than substantial degradation of the SRR material, GFRP laminate or steel bolt. Significant material damage and a distinct failure mode only develop once the connectors are subsequently exposed to fully reversed loading at $R = -1$.

3.2. Evolution of displacement range under water immersion and outdoor aging

Two connectors were submerged in water, and two were exposed to outdoor conditions for a year. Each of the aged connectors are tested under a cyclic load of ±80 kN, as this load condition gives the maximum load range, which is later in Section 4.2, is proven to be the most detrimental loading scenario. Given the limited number of specimens, the available data are sparse, yet they offer useful insights into the potential degradation of the connectors over time.

3.2.1. Stiffness degradation

The relative stiffness degradation of iSRR connectors subjected to different environmental conditions over their fatigue life is presented in Fig. 9. The submerged connectors (red lines) exhibit rapid and pronounced stiffness degradation, reaching failure considerably earlier than both the outdoor-aged connectors and the reference specimens. This early failure suggests a critical vulnerability to prolonged water exposure, likely due to mechanisms such as the swelling of the resin matrix, corrosion of the embedded steel particles, or a weakening of the bond between the SRR piece and the composite component..

The connectors exposed to outdoor conditions (blue curves) exhibit a relative stiffness evolution that closely follows that of the reference specimens (black and grey curves) over most of the fatigue life. In both cases, stiffness remains nearly constant during the initial phase of cycling and begins to decrease gradually after approximately 1.0E10 + 5 cycles. A more pronounced reduction is observed only in the final stage preceding failure, where the outdoor-aged specimens show a slightly earlier onset and a steeper stiffness decline compared to the reference connectors. Overall, the stiffness degradation trends of the outdoor-aged and reference specimens remain comparable up to the late stages of the fatigue process.

3.2.2. Failure modes under cyclic loading

Notably, the failure mode of the submerged connectors is characterized by debonding between the SRR piece and the GFRP facing, along with the crushing of SRR material beneath the embedded nuts. It is also important to keep in mind that this type of submerged connectors is not realistic considering the presence of free edges in the GFRP deck that accelerates the water uptake thereby eventually causing damage to the material and the interfaces. The presence of free edges is a result of cutting the GFRP deck in the required dimension and if eliminated can help minimize the water uptake.

The failure mode for the outdoor-aged connectors, similar to that of the submerged connectors, involves debonding between the SRR piece and the GFRP facing, as well as crushing of the SRR material beneath the embedded nuts as shown in Fig. 11(a). However, the extent and timing of this damage are less severe and occur much later compared to the submerged connectors, which implies that outdoor exposure does not exert the same level of stress on the connectors' internal bonding as direct water immersion.

Fig. 12 shows the condition of the composite deck with iSRR connectors after one year of submersion in water. The black lines indicate the visible extent of water ingress into the composite material. The significant weight gain observed during the submersion period suggests a high level of water absorption, likely affecting the interface between the SRR and the GFRP facing. This water penetration could have weakened the adhesive bond and compromised the structural integrity of the interface, potentially contributing to the observed failure modes under subsequent loading.

4. Discussion on shear fatigue endurance across load ratios and exposure conditions

4.1. Extrapolation methods for F-N curve prediction

To compare all tests on a common fatigue basis, including the specimens tested at $R = 0.1$ and $R = 0.5$ that were stopped after 1.50E + 06 cycles without reaching failure, a displacement-based serviceability criterion is adopted to define the fatigue life of each connector. In this study, an additional displacement-range increase of 0.3 mm between the GFRP facing and the steel end detail is taken as the apparent fatigue "failure" limit for the slip-resistant behaviour of the iSRR connector. This threshold corresponds to the onset of clearly detectable slip and accelerated stiffness degradation while the ultimate load-carrying capacity remains essentially unchanged, and it is

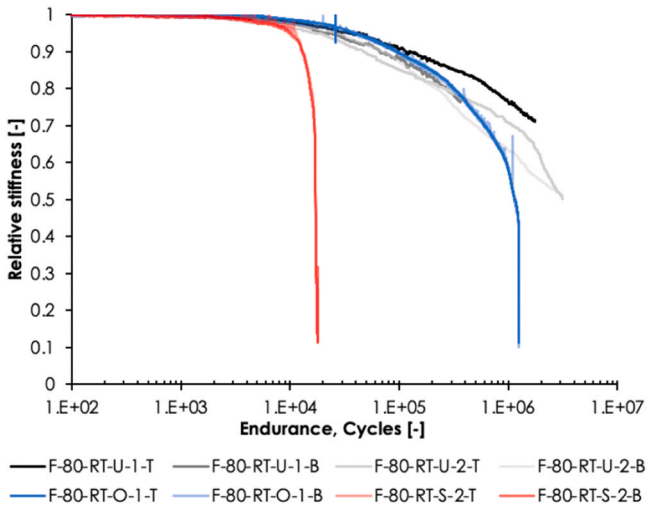

Fig. 10. Relative stiffness of iSRR connector at different cyclic load levels under different environmental exposures.

(a) S-80-RT-S-1-T (b) S-80-RT-S-1-B

Fig. 11. Failure mode of iSRR connectors under cyclic loading after water submersion.

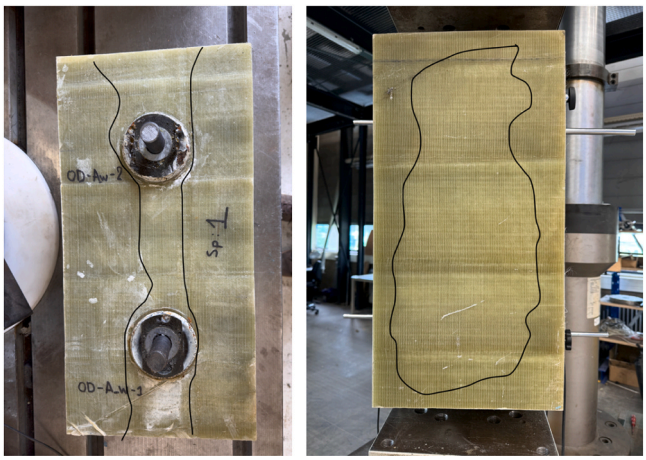

(a) S-80-RT-S-1-T (b) S-80-RT-S-1-B

Fig. 12. Condition of composite deck with iSRR connectors after a year of water submersion and prior to cyclic testing.

consistent both with previous fatigue tests on iSRR connectors [16] and with the 0.3 mm joint-slip limit specified in Annex G of EN 1090-2:2008 for slip-resistant connections [30], which has been used as a serviceability/failure criterion for injected bolted joints in pultruded FRP laminates and steel-FRP joints [31].

To construct the *F-N* curves, the number of cycles required for each connector to reach a displacement-range increase of 0.3 mm is estimated by extrapolating the measured displacement-range evolution. Two extrapolation strategies, previously developed and validated for iSRR connectors in earlier [16], are employed. Only a brief summary is provided here; the full description and reliability assessment of the methods can be found in [16].

4.1.1. Linear regression method

In the first approach, the displacement-range increase is plotted as a function of the number of cycles in a log-log diagram. For each connector, a subset of the data is selected such that the evolution can be represented accurately by a single trend line. Data points in the very late stage of loading, where the degradation rate decreases and may introduce curvature, are excluded to maintain a high coefficient of determination; in this study, an R^2 threshold of 0.97 is adopted. A linear regression is then fitted to the remaining points, and the resulting power-law relationship is used to extrapolate the number of cycles at which the displacement-range increase would reach the 0.3 mm limit. This procedure provides a relatively accurate estimate of fatigue life while remaining computationally simple.

4.1.2. Elbow (segmented regression) method

The second approach recognises that, for many connectors, the displacement-range increase does not follow a single slope but exhibits successive stages with different degradation rates. To capture this behaviour, the data are segmented before applying linear regression. The optimal number and position of breakpoints are identified using an "elbow" analysis of the sum of squared errors for different segmentations. For each candidate number of segments, linear models are fitted to the segments, and the corresponding sum of squared errors is computed; the elbow point in this curve is taken as the best compromise between model accuracy and complexity. The resulting segments typically reflect the fast-slow-fast pattern of degradation observed in the experiments. For each connector, the segment with the highest slope (i.e. the most severe degradation rate) is then extrapolated to the 0.3 mm threshold, providing a conservative estimate of the number of cycles to reach the serviceability limit.

Previous work [16] has shown that the linear regression method tends to give less conservative predictions, with good agreement with the actual cycles to failure, whereas the elbow method provides lower, more conservative fatigue-life estimates. In the present study, both methods are applied to the new dataset, and the resulting cycle counts are used to construct the unified *F-N* curve for the iSRR connector.

4.2. Influence of R ratio

An evaluation is performed on the effect of different load ratios on fatigue degradation, specifically focusing on the increase in additional displacement range. For a more robust evaluation, the extrapolation methods described in [16] are used to create and examples of the projection of the displacement range increase in log-log scale are presented for the specimens tested under three different R ratios in Fig. 13. The number of cycles necessary to reach the 0.3 mm displacement range increase threshold criterion is extrapolated using both the linear regression and the elbow method described earlier and the results are detailed in Table 5.

Notable differences in extrapolated fatigue life are observed between top (T) and bottom (B) connectors within the same specimen. These differences are primarily attributed to the inherent stochastic nature of fatigue, local microstructural features and panel-specific asymmetries, such as variations in the SRR filling and the proximity of the bottom facing to the internal webs of the GFRP sandwich panel.

Additionally, this variability highlights the limitations of relying on a single, deterministic prediction for fatigue life. When evaluating hybrid GFRP-steel connections, focusing only on the average performance of a specimen can be misleading. Instead, it is more realistic to derive design values from the statistical distribution of every individual connection point. By treating each connector as an independent data point, the weakest link behaviour of the assembly is more accurately captured. This approach ensures that the resulting design curves and serviceability limits are robust enough to account for the unavoidable scatter caused by real-world assembly conditions and inhomogeneous material properties.

The connectors tested at $R = 0.5$ show a much slower progression toward failure, compared to connectors tested at the same maximum load with load ratio of $R = -1$. These connectors endure a far greater number of cycles before reaching 0.3 mm of displacement range increase, indicating a better fatigue performance under the $R = 0.5$ conditions. The displacement range increases more gradually, implying that this load ratio subjects the connectors to less severe fatigue damage. The $R = 0.1$ connectors exhibit intermediate behaviour. Their displacement range increase is faster than at $R = 0.5$, but slower than for $R = -1$. This suggests that while $R = 0.1$ still leads to noticeable fatigue damage, it is less damaging than fully reversed loading but more harmful than positive loading with $R = 0.5$.

Fig. 14 illustrates the log-log relationship between the number of cycles (x-axis) and the maximum applied force (y-axis) for three different R values: −1, 0.1, and 0.5. All the curves start at 120 kN on the y-axis, which corresponds to the slip resistance of the iSRR connectors. This is because if the connector were subjected to a maximum force of 120 kN, slip would occur almost immediately, and the 0.3 mm displacement range increase would be reached within the first cycle. This starting point serves to illustrate the limiting condition of the iSRR connector's performance, with lower applied forces requiring more cycles to reach the failure threshold. Additionally, results from [2] are utilized to provide more data for accurate estimation for $R = -1$. All the plotted points, except at 120 kN, represent averages of linearly extrapolated fatigue lives from top/bottom connectors per maximum force level.

The slope of the curves demonstrates how the fatigue life decreases as the maximum applied force increases, with the load ratio influencing the rate of this reduction, indicating the influence of different load ratios on the rate of fatigue degradation. As expected, the $R = -1$ curve exhibits the steepest slope, suggesting that under fully reversed loading

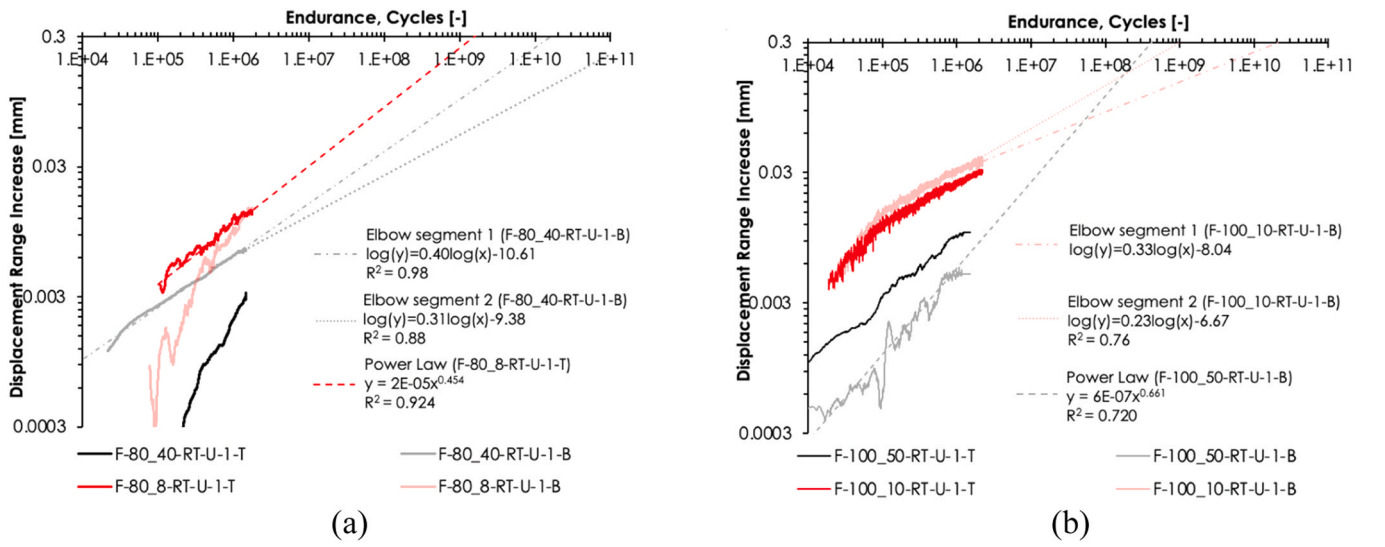

Fig. 13. Connectors' displacement range increase in logarithmic scale axes under different R ratios: (a) Maximum load of 80 kN, (b) Maximum load of 100 kN.

Table 5
Estimation of cycle counts until failure criterion with different R ratios.

Connector's ID	Parameter	Linear regression	Elbow method $log\ (y) = A + B \cdot log\ (x)$		
		$y = A \cdot x^B$	Segment 1	Segment 2	Segment 3
F−80_8-RT-U−1-T	A	2.00E−05	−10.62	−8.51	-
	B	0.454	0.44	0.29	-
	R^2	0.924	0.93	0.69	-
	Cycles at 0.3 mm	1.59E + 09	1.79E + 09	6.56E + 10	-
F−80_8-RT-U−1-B	A	5.00E−08	−14.75	−15.04	−11.94
	B	0.876	0.73	0.75	0.53
	R^2	0.945	0.85	0.83	0.71
	Cycles at 0.3 mm	5.47E + 07	1.13E + 08	1.04E + 08	5.33E + 09
F−100_10-RT-U−1-T	A	9.00E−06	−8.83	−7.67	−7.49
	B	0.619	0.34	0.29	0.27
	R^2	0.945	1	0.97	0.93
	Cycles at 0.3 mm	2.00E + 07	1.37E + 09	5.90E + 09	8.48E + 09
F−100_10-RT-U−1-B	A	3.00E−06	−8.04	−6.67	-
	B	0.75	0.33	0.23	-
	R^2	0.964	0.99	0.76	-
	Cycles at 0.3 mm	4.60E + 06	9.12E + 08	1.83E + 10	-
F−80_40-RT-U−1-T	A	8.00E−10	−12.2	−30.23	-
	B	0.947	0.4	1.67	-
	R^2	0.63	0.17	0.21	-
	Cycles at 0.3 mm	1.54E + 09	1.21E + 12	3.39E + 07	-
F−80_40-RT-U−1-B	A	3.00E−05	−10.61	−9.38	-
	B	0.38	0.4	0.31	-
	R^2	0.893	0.98	0.88	-
	Cycles at 0.3 mm	3.34E + 10	1.56E + 10	2.78E + 11	-
F−100_50-RT-U−1-T	A	1.00E−05	−10.8	−9.34	-
	B	0.487	0.44	0.34	-
	R^2	0.95	0.97	0.84	-
	Cycles at 0.3 mm	1.53E + 09	2.57E + 09	2.37E + 10	-
F−100_50-RT-U−1-B	A	6.00E−07	−11.51	−7.15	-
	B	0.661	0.44	0.13	-
	R^2	0.72	0.76	0.3	-
	Cycles at 0.3 mm	4.20E + 08	1.64E + 10	2.11E + 19[1]	

1) Value obtained from extrapolation of the regression model. Due to the very small slope of the fitted segment, the predicted cycle count exceeds practical engineering ranges and should therefore be interpreted with caution.

conditions, the connectors experience the most rapid degradation in their fatigue life. This behaviour is attributed to the reversal of stress in each cycle, which intensifies fatigue damage by subjecting it to alternating compressive and tensile stresses. Consequently, the fully reversed load ratio induces greater damage accumulation compared to other load ratios, where the stress amplitudes are lower.

Conversely, the curves for positive load ratios, particularly $R = 0.5$, show much gentler slopes, implying that these loading conditions impose less severe fatigue damage on the connectors. The flatter the slope, the greater the number of cycles the connectors can endure before reaching the failure threshold of 0.3 mm displacement range increase. This aligns with the expectation that lower amplitude loading cycles (higher R values) allow for an extended fatigue life.

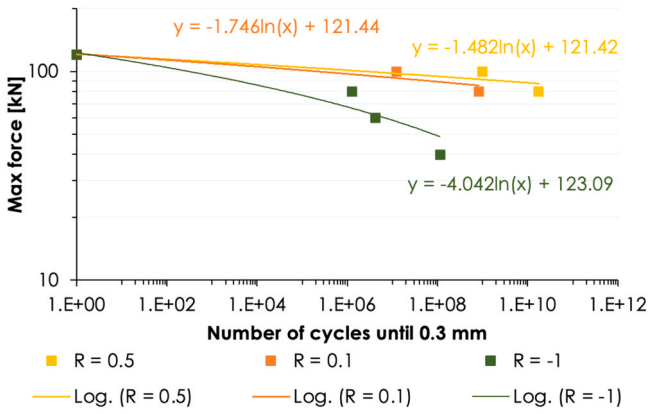

Fig. 14. Influence of R ratio on the fatigue life of the connectors under shear loading.

4.2.1. *Unified F-N curve*

To account for the experimental scatter observed between individual connectors, the fatigue life is analysed through a unified statistical framework. This approach ensures that the localized variations in performance are captured within a reliable characteristic relationship. Specifically, a unified *F-N* is constructed utilising the same regression-based approach previously applied to fatigue results if iSRR connectors with $R = -1$ in an earlier study [16]. The methodology is applied to the combined dataset including all R ratios, enabling the construction of a unified *F-N* curve that captures the fatigue behaviour of the iSRR connector independently of mean load effects. A brief summary of the method is provided below for completeness.

The relationship between the number of cycles required to reach the 0.3 mm displacement-range criterion and the applied force range is represented using a linear fit on a log-log scale, in accordance with the procedure described in ASTM E739 [32]. After transforming the variables, the *F-N* relationship is expressed in the form:

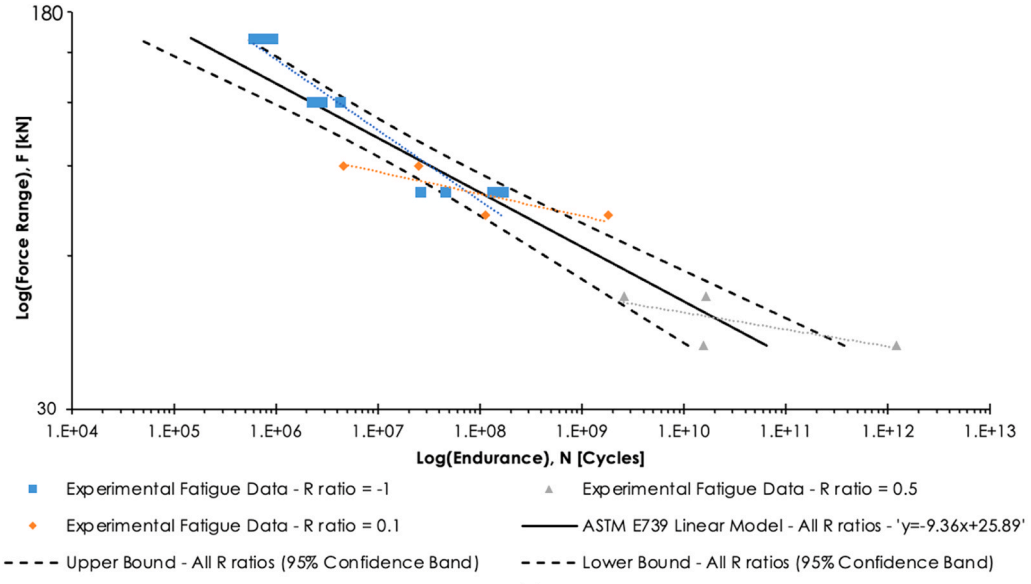

(a)

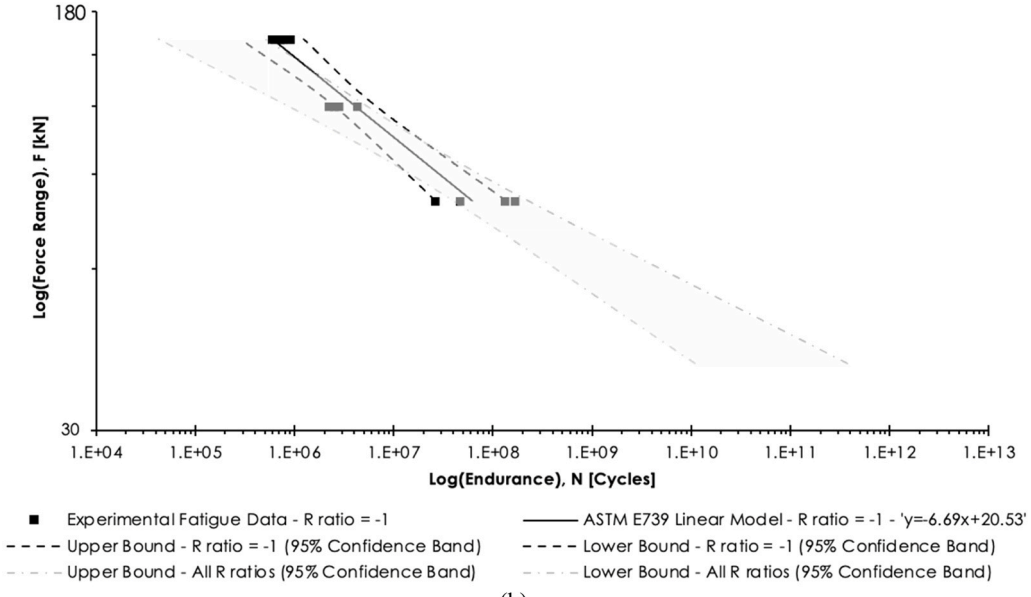

(b)

Fig. 15. Comparison between different fatigue performance analysis: (a) All R ratios and (b) R = −1 taken from [16].

$$\log(N) = A + B \cdot \log(Fmax)$$

where A and B are obtained through linear regression. The confidence bounds around the regression line are calculated following the statistical procedure outlined in [32] accounting for the number of specimens, the scatter in the data, and the distribution of force levels.

In Fig. 15(a), all the data are plotted irrespective of the R ratio, allowing a statistical analysis across the entire dataset. The regression line and confidence bands are obtained for all the data to provide an overall trend. The force range is chosen as an appropriate y-axis parameter for describing the fatigue performance, considering the diversity of R ratios applied.

The comparison between Fig. 15(a) and Fig. 15(b) aims to highlight the implications of incorporating multiple load ratios in the fatigue analysis, particularly in terms of improving the accuracy of fatigue life predictions. When only the $R = -1$ data is considered, a different fatigue behavior emerges compared to the more comprehensive dataset. Observations from Fig. 15(b) indicate that relying solely on the $R = -1$ dataset could result in an overprediction of the connector's resistance at higher load levels. Meanwhile, using $R = -1$ data alone would provide underestimated number of cycles and reduced confidence at lower load levels, owing to the variability and broader scatter of experimental results. Including data from different R ratios provides an improved statistical basis, contributing to a more reliable estimation of the connector's fatigue performance. This highlights the advantage of considering multiple R ratios when evaluating connector behavior under realistic service conditions.

The curves plotted in Fig. 15(a) and Fig. 15(b) further demonstrate that the slope of the regression line changes significantly depending on the dataset considered. For the unified approach, so for all R ratios, the slope is steeper at −9.36, which suggests a quicker decline in fatigue life with increasing load range compared to the −6.69 slope at $R = -1$. This difference reflects how an *F-N* curve based only on fully reversed loading may not be the most damaging condition for the highest load ranges, contrary to what was initially expected.

By creating an *F-N* curve that includes every R ratio, the design and engineering procedures are simplified. Including separate *F-N* curves for every different R ratio can be complicated in practical design verifications, especially when calculating fatigue life under varying conditions. Therefore, the recommendation for engineering practice is to start with the unified *F-N* curve for an iSRR connector as it encompasses data from all R ratios and provides a reasonable estimation of fatigue life. If more precision is needed, separate R ratio-specific curves could then be used for more detailed damage analysis. This approach balances simplicity with sufficient accuracy, as analysis conducted on structural level variations due to traffic loads indicated that the unified *F-N* curve is adequate and does not lead to overestimation of fatigue life.

Finally, this unified *F-N* curve derived in this study should be interpreted as a characteristic relationship for the specific connector-deck system investigated here, namely M27 iSRR connectors embedded in the tested GFRP sandwich web-core deck, manufactured from the same vacuum-infused panels and installed with the same detailing and preload, under room-temperature conditions and the range of load ratios and force ranges considered ($R = -1$, 0.1, 0.5; F_{max}=40–100 kN). The analysis is based on nominal material and geometric properties, without an explicit probabilistic treatment of variability or size effects.

Regarding scalability, it is anticipated that the current results remain valid, and potentially conservative, for larger connector dimensions. An increase in connector size implies a larger SRR volume and a greater interface area for potential damage to distribute across, which typically enhances fatigue resistance by reducing local stress concentrations. Conversely, applying these results to smaller dimensions, where the reduced interface area and material volume would lead to higher damage density, should be done with caution. Therefore, the direct use of this *F-N* curve for smaller connector geometries, different laminate configurations, or temperature regimes (e.g., close to or above the resin glass-transition temperature) should be ideally supported by additional calibration or appropriate safety factors.

4.3. Influence immersion and outdoor aging

The fatigue life extrapolation for iSRR connectors subjected to one year of environmental aging is extrapolated based on the two methods presented in Section 4.1. Fig. 16 displays the displacement range increase of iSRR connectors tested at a consistent load level of ±80 kN, with the different colours representing connectors subjected to distinct environmental conditions.

Interestingly, the connectors aged outdoors exhibit a displacement range increase that is very similar to the reference connectors tested at room temperature. This suggests that the outdoor exposure, while slightly affecting the connector performance, did not drastically reduce fatigue resistance compared to the non-aged connectors. Both blue and the black lines show a more gradual increase in displacement range compared to the submerged connectors. However, between the reference (blue) and the outdoor-aged (black) connectors, the reference connectors seem to perform slightly better, displaying a slightly slower rate of displacement range increase, indicating a marginally greater resistance to fatigue.

On the other hand, the submerged (red) connectors display the fastest displacement range increase, indicating accelerated stiffness degradation and earlier failure compared to both the outdoor-aged and the reference connectors. This implies that water exposure has a more detrimental impact on the fatigue performance of the connectors, leading to a significant reduction in fatigue life. The submerged connectors reach the 0.3 mm failure criterion much earlier, around 2.00E + 4 cycles, whereas the outdoor-aged connectors and the reference connectors demonstrate a more gradual progression, reaching the 0.3 mm failure criterion closer to 7.50E + 05 cycles, as shown in parentheses in Table 6.

These results highlight that outdoor exposure has a less drastic effect on the fatigue performance compared to submersion. Importantly, considering the intended application of these connectors in bridge structures, where they will always be in non-submerged conditions, the outdoor exposure results are particularly relevant. The study involving submerged conditions was conducted to evaluate the worst-case scenario, ensuring comprehensive safety margins. Given the promising results observed in the outdoor-aged connectors, it is evident that the iSRR connectors exhibit sufficient resilience for bridge environments, where occasional wetting due to rain or moisture is expected, but continuous submersion is not. These findings support the reliability of the connectors under realistic field conditions, highlighting their suitability for practical use in infrastructure subjected to typical outdoor aging factors.

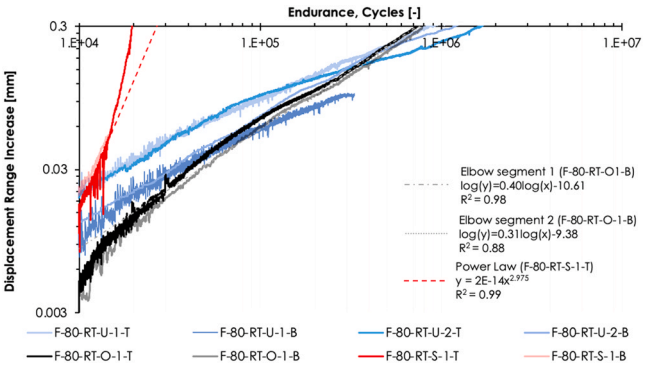

Fig. 16. Recorded connectors' displacement range increase in logarithmic scale axes under different environmental exposure conditions.

Table 6
Estimation of cycle counts until failure criterion with different R ratios.

Connector's ID	Parameter	Linear regression	Elbow method $log\ (y) = A + B \cdot log\ (x)$		
		$y = A \cdot x^B$	Segment 1	Segment 2	Segment 3
F−80-RT-S−1-T	A	2.00E−14	−35.79	−18.83	−41.23
	B	2.975	3.51	1.59	4
	R^2	0.99	0.93	0.84	0.97
	Cycles at 0.3 mm (−1.95E+04)*	2.69E + 04	1.92E + 04	6.31E + 04	2.19E + 04
F−80-RT-S−1-B	A	3.00E−09	−62.23	−73.29	-
	B	1.728	6.17	7.29	-
	R^2	0.741	1	1	-
	Cycles at 0.3 mm (−1.96E+04)*	4.26E + 04	2.02E + 04	1.98E + 04	-
F−80-RT-O−1-T	A	5.00E−06	−12.09	−12.35	-
	B	0.821	0.81	0.83	-
	R^2	0.998	0.99	1	-
	Cycles at 0.3 mm (7.30E+05)*	8.46E + 05	7.10E + 05	7.33E + 05	-
F−80-RT-O−1-B	A	1.00E−06	−12.42	−12.71	-
	B	0.924	0.83	0.85	-
	R^2	0.996	0.99	1	-
	Cycles at 0.3 mm (7.99E+05)*	6.61E + 05	7.80E + 05	8.11E + 05	-

* Number of cycles that actually reached the 0.3 mm failure criterion

5. Concluding remarks

This study investigated the fatigue and hygrothermal performance of iSRR connectors embedded in GFRP sandwich web-core panels. A total of 12 connectors were tested under different R ratios and environmental exposure conditions using a dual-connector shear test setup. Eight specimens were subjected to cyclic loading at $R = 0.1$ and $R = 0.5$ and compared with twelve fully reversed ($R = -1$) tests reported in previous work. Four additional connectors were conditioned for one year, two through full water immersion and two through outdoor aging, to evaluate long-term environmental effects. To ensure representativeness, all connectors were installed in full-scale GFRP sandwich panels with geometric dimensions consistent with those expected in actual bridge deck renovation projects.

For a number of specimens where it was feasible, fatigue testing was continued until failure, enabling direct observation of the mechanisms governing damage evolution and fracture of the connection under cyclic shear loading. Based on the experimental results and analysis, the following key conclusions can be drawn:

- A unified *F-N* curve developed by combining fatigue data from all R ratios resulted in a regression slope of −9.36, which is marginally flatter than the slope obtained using exclusively the $R = -1$ dataset (−6.6). This consistency across loading conditions supports the use of a single fatigue design curve for the iSRR connector. However, the proposed unified *F-N* curve is applicable to M27 iSRR connectors in the tested GFRP sandwich deck configuration and loading regime, and its extension to significantly different connector or deck designs should be accompanied by additional verification.
- The influence of one year of environmental exposure was examined by testing connectors submerged in water and connectors aged outdoors. The submerged specimens exhibited rapidly accelerated stiffness degradation, reaching the failure criterion at approximately 2.00E + 04 cycles, in contrast to the outdoor-aged and reference specimens, which failed at around 7.50E + 05 cycles. This highlights the markedly detrimental effect of prolonged water immersion, whereas outdoor exposure had only a minimal influence on fatigue resistance.
- Across all examined cases, cyclic damage was governed primarily by debonding of the SRR injection from the oversized hole in the lower GFRP facing and local compressive damage of the SRR material ahead of the embedded bolt and nut. These failure mechanisms occurred irrespective of prior environmental conditioning or low-range cyclic loading prior to the high-range cyclic loading, indicating that the fundamental fracture process is intrinsic to the connector's shear transfer mechanism.

These findings demonstrate that the iSRR connector possesses a robust fatigue response, with performance largely governed by load range rather than mean load or environmental variations under typical service conditions. The strong alignment of behaviour across R ratios, the consistency of failure mechanisms, and the favourable performance of outdoor-aged specimens all support the suitability of the connector for structural applications subjected to cyclic loading. Importantly, since the intended use of these connectors is in bridge systems that remain in non-submerged environments, the negligible impact of outdoor aging provides confidence in their long-term reliability and durability in realistic field conditions.

CRediT authorship contribution statement

Marko Pavlovic: Writing – original draft, Supervision, Resources, Project administration, Funding acquisition, Conceptualization. **Angeliki Christoforidou:** Writing – original draft, Visualization, Validation, Methodology, Investigation, Data curation. **Abishek Baskar:** Writing – original draft, Methodology, Investigation, Data curation.

Declaration of Competing Interest

The authors declare that they have no known competing financial interests or personal relationships that could have appeared to influence the work reported in this paper.

Acknowledgements

The authors extend their gratitude to the Dutch Ministry of Infrastructure, Rijkswaterstaat, whose generous financial support proved pivotal in the successful completion of this research. The valuable contribution of AOC Resins is appreciated, since they graciously provided the material which significantly aid the progression of our work.

Data availability

Data will be made available on request.

References

[1] K. Gkoumas, et al., Research and Innovation in Bridge Maintenance. Inspection and Monitoring, 2019.
[2] M. Artus, C. Koch, State of the art in damage information modeling for RC bridges–A literature review, Adv. Eng. Inform. 46 (2020) 101171.
[3] S. KÜttenbaum, et al., Reliability and partial factor-based assessment of a highway bridge supported by nondestructive testing, Struct. Concr. 26 (5) (2025) 5535–5554.
[4] H. Klatter, A. Vrouwenvelder, J. van Noortwijk, Societal aspects of bridge management and safety in the Netherlands. Proceedings of the Third International Conference on Bridge Maintenance, Safety and Management (IABMAS), Porto, Portugal, 16-19 July 2006, 2006.
[5] A. Zhu, et al., Fatigue test and life evaluation of rib-to-deck connections in orthotropic steel bridge decks, J. Constr. Steel Res. 197 (2022) 107442.
[6] M.F. SÁ, et al., Dynamic behaviour of a GFRP-steel hybrid pedestrian bridge in serviceability conditions. Part 2: Numerical and analytical study, Thin-Walled Struct. 118 (2017) 113–123.
[7] H. Liu, et al., Corrosion fatigue life simulation and reliability analysis of steel structures, J. Constr. Steel Res. 223 (2024) 109075.
[8] T. Keller, Use Fibre Reinf. Polym. Bridge Constr. (2003).
[9] V. Mara, R. Haghani, P. Harryson, Bridge decks of fibre reinforced polymer (FRP): A sustainable solution, Constr. Build. Mater. 50 (2014) 190–199.
[10] M. Poulton, S. Wendel, Modular FRP-steel bridges for the UK road network, Struct. Eng. 103 (9) (2025) 10–18.
[11] H.-Y. Kim, S.-M. Kim, Y.-K. Hwang, Des. a pultruded GFRP Deck. Highw. Bridges (2003).
[12] P.S. Valvo, E. Davini, R. Fabio, The European project SUREBridge-Analysis of a case study bridge. Proceedings of the 33rd International CAE Conference and Exhibition, EnginSoft SpA,, 2017.
[13] E. Davini, et al., Il progetto SUREBridge/The SUREBridge project, COMPOSITI Mag. 13 (47) (2018) 8–14.
[14] Europe, F. *InfraCore® technology: The solution to delamination in composite*. Available from: ⟨https://www.fibercore-europe.com/en/composite-as-a-structural-material/infracore-technology/⟩.
[15] F. Csillag, Demountable deck-to-girder connection of FRP-steel hybrid bridges, Delft Technical University,, 2018.
[16] A. Christoforidou, M. Pavlovic, Fatigue performance of composite-steel injected connectors at room and elevated temperatures, Eng. Struct. 315 (2024) 118421.
[17] A. Christoforidou, Fatigue behavior of steel reinforced resin connectors for fibre-polymer composite bridge decks, Delft University of Technology,, 2025.
[18] A. Christoforidou, et al., *Fatigue performance of injected steel reinforced resin connectors in GFRP sandwich web core panels* in *11th International Conference on Fiber-Reinforced Polymer (FRP) Composites in Civil Engineering (CICE 2023)*, Zenodo,, Rio de Janeiro, Brazil, 2023.
[19] G. Olivier, et al., Feasibility of bolted connectors in hybrid FRP-steel structures, Constr. Build. Mater. 383 (131100) (2023).
[20] M. Shakiba, et al., Short-term durability of GFRP stirrups under wet-dry and freeze–thaw cycles, Constr. Build. Mater. 398 (2023) 132533.
[21] J.H. Kim, et al., Experimental investigation of freeze-thaw environmental effects on the fatigue life of CFRP composites, Polym. Test. 143 (2025) 108702.
[22] J.V.R. Swinnen, Modelling the mechanical performance of bolted deck-to-girder connections in FRP-steel hybrid bridges, Delft University of Technology,, 2020.
[23] H. Tuwair, et al., Evaluation of sandwich panels with various polyurethane foam-cores and ribs, Composites Part B Engineering 79 (2015) 262–276.
[24] *Airblast-Abrasives B.V., High carbon steel shot & grit: Technical data sheet.*
[25] *AOC Resins. Technical Data Sheet: Daron® 8151 Resin (Marketed as AQR 1025/B25)*. 2021.
[26] A. Christoforidou, R. Verleg, M. Pavlovic, Static, fatigue and hygroscopic performance of steel-reinforced resins under various temperatures, Constr. Build. Mater. 403 (2023) 133079.
[27] A. Christoforidou, et al., Compressive behaviour and micromechanical modelling of steel-reinforced resin under monotonic and cyclic loading, Compos. Sci. Technol. (2025) 111387.
[28] CUR, *CUR96: CUR Recommendation 96: Fibre Reinforced Polymers in Civil Load Bearing Structures*. 2003, CUR Amsterdam, The Netherlands.
[29] K. Gribnau, Shear force in bolted connections for hybrid steel-FRP bridges, Delft University of Technology,, 2021.
[30] C. EN, 1090-2: execution of steel structures and aluminium structures–part 2: technical requirements for steel structures, European Committee for Standardisation,, Brussels, 2008.
[31] B. Zafari, et al., Static and fatigue performance of resin injected bolts for a slip and fatigue resistant connection in FRP bridge engineering. Structures, Elsevier,, 2016.
[32] ASTM, *E739 10 Standard Practice for Statistical Analysis of Linear or Linearized Stress-Life*, Annu. Book ASTM Stand. (1980).